Current-induced depairing in the Bi_{2}Te_{3}/FeTe interfacial superconductor

M. N. Kunchur, C. L. Dean, N. Shayesteh Moghadam, J. M. Knight, Q. L. He, H. Liu, J. Wang, R. Lortz, I. K. Sou, and A. Gurevich

Phys. Rev. B **92**, 094502 — Published 1 September 2015

DOI: 10.1103/PhysRevB.92.094502

Current-induced depairing in the Bi_2Te_3/FeTe interfacial superconductor

M. N. Kunchur,* C. L. Dean, N. Shayesteh Moghadam, and J. M. Knight
Department of Physics and Astronomy, University of South Carolina, Columbia, SC 29208, USA

Q. L. He, H. Liu, J. Wang, R. Lortz, and I. K. Sou
William Mong Institute of Nano Science and Technology,
the Hong Kong University of Science and Technology, Hong Kong, China

A. Gurevich
Department of Physics, Old Dominion University, Norfolk, Virginia 23529, USA
(Dated: August 12, 2015)

We investigated current induced depairing in the Bi_2Te_3/FeTe topological insulator-chalcogenide interface superconductor. The measured depairing current density provides information on the magnetic penetration depth and superfluid density, which in turn shed light on the nature of the normal state that underlies the interfacial superconductivity.

PACS numbers: 74.25.fc, 74.25.Sv, 74.70.Xa, 74.78.Fk

I. INTRODUCTION

Topological insulators (TI) and interface superconductors are both topics of intense current interest[1]. The surface states of a TI represent a novel 2D conducting system with very high normal conductivity because of protection against time-reversal invariant scattering mechanisms. Besides systems that are 2D because of intrinsic reduced dimensionality (e.g., ultrathin films or graphene), superconductivity confined to the interface layer where two bulk systems meet represents another novel 2D system. Understanding the nature and origin of the charge carriers that underlie this superconductivity is therefore a matter of primary interest, besides obtaining knowledge of the fundamental parameters that characterize these systems, and exploring novel and exotic phenomena that these new systems hold.

The interface of the Bi_2Te_3/FeTe heterostructure represents the first realization of superconductivity at the interface between a topological insulator (Bi_2Te_3) and an iron-chalcogenide (FeTe), with neither system a superconductor by itself[2]. While the cause of this superconductivity was not conclusively determined in that work, they suggested the possibility that the robust topological surfaces states (TSS) may be doping the FeTe and suppressing the antiferromagnetism in a thin region close to the interface, thus inducing the observed 2D superconductivity. Indeed, their observations of certain signatures of the Berezinski-Kosterlitz-Thouless (BKT) transition, a square-root temperature dependence of the parallel upper critical field, and other observations conclude that the 2D superconductivity resides in a 7 nm thick layer near the interface that is very likely to be within the FeTe. Our studies of the vortex explosion phenomenon in this system also confirm a superconducting layer thickness in the 7-8 nm range[3]. In their work, He et al. grew a variety of Bi_2Te_3/FeTe heterostructures with varying thicknesses of the Bi_2Te_3 top layer and found that the critical transition temperature T_c reaches a plateau beyond about 6 quintuple layers, roughly 6 nm, which agrees with the 5 nm thickness of the TI for which the TSS are fully developed[2]. In other work[4], directional point-contact spectroscopy revealed two gaps, with a large isotropic gap associated with a thin FeTe layer adjacent to the interface, and a small anisotropic gap associated with proximity-induced superconductivity in the Bi_2Te_3 TI itself.

Along with T_c and the upper-critical magnetic field B_{c2}, the depairing (pair-breaking) current density j_d represents one of the principal critical parameters of a superconductor. Of the three, j_d is the most difficult quantity to measure and therefore has not been measured in the vast majority of superconductors. A combined knowledge of B_{c2}, j_d, and the normal-state resistivity ρ_n provides a window to the in-plane magnetic penetration depth λ, superfluid density n_s, and the normal-carrier scattering time τ.

This work used fast pulsed-signal techniques to perform, to our knowledge, the first measurement of j_d in the Bi_2Te_3/FeTe topological insulator-chalcogenide interface superconductor. As shown in our earlier work[5], this j_d in combination with B_{c2}, provides a reliable transport based estimation of λ that is not vulnerable to errors arising from magnetism, which affect magnetic-induction based methods for measuring λ. The indirect information obtained about n_s and τ, sheds new light on the nature of the normal state that underlies the interface superconductivity.

II. EXPERIMENTAL DETAILS

The samples were synthesized by a VG-V80H MBE system, and consist of a ZnSe buffer layer (50 nm) deposited on a GaAs (001) semi-insulating substrate, followed by a deposition of 220 nm thick FeTe, which is then capped with a 20 nm thick Bi_2Te_3 layer

(This thickness comprises 20 QLs, i.e., quintuple layers. The Bi_2Te_3 unit cell consists of 3 QLs bonded by van der Waals forces along the [0001] direction.) Upper-critical-field measurements[2] and vortex-explosion measurements[3] show that the superconductivity occurs within a 7 nm thick interfacial layer, which is much thinner than both the FeTe and Bi_2Te_3 layers. The properties of this interface layer are not strongly related to the individual thicknesses of the FeTe and Bi_2Te_3 layers, as long as the Bi_2Te_3 is thicker than $\gtrsim$ 5 nm; below this, the TSS start to degrade due to the hybridization of the top and bottom surfaces, which in turn can affect the properties of the superconducting interface. This has been studied systematically in the earlier work by He et al.[2]. Samples were stored under vacuum to protect from oxidation. The Bi_2Te_3/FeTe heterostructure is effectively electrically insulated from the ZnSe and GaAs; however, the FeTe provides a relatively resistive parallel path to the superconducting interface, which results in a small correction to the normal-state conductivity of the interface layer.

In the previous work[2], the measurements were conducted on 0.5 mm × 2 mm unpatterned strips that were cut out using a diamond scribe. The present work utilized projection photolithography followed by argon-ion milling to pattern narrow microbridges optimized for the high current-density pulsed four-probe measurements conducted in this work. In this geometry, the contacts are located a considerable distance from the bridge and are connected to the bridge by tracks that are much wider than the bridge itself. This ensures a uniform current distribution in the bridge. Two bridges, samples A and B, were studied with lateral dimensions of width $w = 11.5$ μm and length $l = 285\mu$m, and $w = 12$ μm and $l = 285\mu$m, respectively. The onset T_c (defined as the intersection of the extrapolation of the normal-state portion and the extrapolation of the steep transition portion of the $R(T)$ curve) for both bridges was 11.7 K. Further details about sample preparation are provided elsewhere[2].

The cryostat was a Cryomech PT405 pulsed-tube closed-cycle refrigerator. All measurements were made in zero applied magnetic field. While the very low reference curves at $I \lesssim 60$ μA were measured using continuous DC signals, the main electrical transport measurements were made with pulsed signals using in-house built pulsed current sources, preamplifier circuitry, and a LeCroy model 9314A digital storage oscilloscope. The pulse durations were in the 0.1–5 μs range with a pulse repetition frequency of ∼1 Hz (duty cycles of ∼1 part per 10^6). This reduces Joule heating of the sample to the the mK range, as was ascertained by a direct measurement of the thermal resistance $\Delta T/\Delta P \approx 0.4$ K/W using the method devised in our previous work[6]. About 100 pulses were averaged to improve the signal-to-noise ratio.

For curves that were measured at a constant and relatively small ($\lesssim$ 40 mA) pulsed-current level, such as the R versus T curves where only T varies from point to point, longer pulses together with a constant high preamplifier gain are used and the data is taken automatically using a computer controlled sequence. The pulsed measurements for I-V curves were conducted manually with the preamplifier gain and exact pulse duration continuously optimized. This tedious and time consuming method makes it possible to attain the depairing current value even at $T \ll T_c$. In our earlier work[7,8] this method provided one of the most extended ($0 \lesssim T \lesssim T_c$) depairing-current measurements made on any superconductor. Contact resistances (< 1 Ω) are much lower than the normal resistance R_n of the bridge, and heat generated at contacts does not reach the bridge within the time duration t of each pulse, since the thermal diffusion distance ($\sqrt{Dt} \sim 10\mu$m) is much shorter than the contact-to-bridge distance (> 1 mm); D is the diffusion constant.

Further details of the measurement techniques have been published in previous review articles[8–10].

III. RESULTS AND DISCUSSION

Fig. 1(a) shows resistive transitions in $B = 0$ at various applied currents. Taking various resistance criteria R_c, as shown by the horizontal dashed lines, one can define the temperature that corresponds to a particular "resistive critical current" as the value where the curve for that particular applied current intersects the respective horizontal line. (As will be discussed later in this section, as T is lowered below T_c the normal-state conductance is nearly temperature independent and dominated by the normal conductance of the interface layer itself; the parallel conductance of the FeTe layer, which has a negative $R(T)$ slope, provides a diminishing contribution below T_c.) Plotting these currents and temperatures for each criteria, as $I^{2/3}$ vs T and simply I vs T, results in Fig. 1(b) and (c) respectively. As can be seen, there is a threshold around $T \approx 10$ K below which the data follow the classic $I^{2/3} \propto T$ behavior expected for the temperature dependence of the depairing current (Fig. 1(b)); above 10 K, a linear $I \propto T$ behavior is followed (Fig. 1(c)). Fig. 2 shows a similar set of plots for sample B; the threshold temperature is seen to be around 10.2 K. This cross over in the power law occurs at a temperature that appears to be close to the T_{BKT} found by He et al.[2].

There are several possibilities for this cross over. With increasing current, resistance appears in a superconductor at zero external magnetic field chiefly through the two processes of pair breaking and flux flow associated with the perpendicular component of self field of the applied current. The self field has the profile $B^{\perp}_{\rm self}(x) = [\mu_0 I/2\pi w] \ln[(w+2x)/(w-2x)]$ across the width of the bridge (origin taken at the center of the bridge), with the logarithmic divergence cut off by the film thickness to $B^{\perp}_{\rm self}(\pm w/2) = (\mu_0 I/2\pi w) \ln(w/d)$. Even this edge field is only ∼10 mT, which is dwarfed by B_{c2} and even

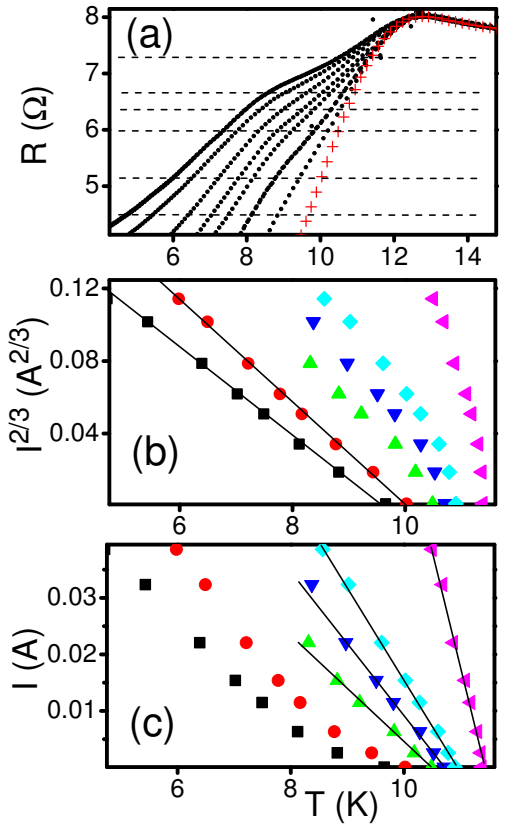

FIG. 1: *(a) Resistive transitions for sample A in zero magnetic field at transport current values of (left to right): 38.6, 32.4, 22.1, 15.4, 11.5, 6.34, 2.57, 0.0534 mA. The lowest current (red crosses) is continuous DC; the remaining currents are pulsed. (b) Two-thirds power of the applied current versus the temperature where the curves in upper panel are intersected by the horizontal dashed lines defining the following normalized-resistance criteria: R_c/R_n =0.56, 0.64, 0.75, 0.83, and 0.91 (where R_n is the normal-state resistance). (c) The applied currents plotted linearly against the same temperatures as in middle panel. Straight lines are guides to the eye.*

exceeded by the lower critical field B_{c1} over most of the temperature range, so that pair breaking dominates over flux dissipation. However the opposite is true closer to T_c where the self field of the fixed current I will exceed B_{c1} and lead to appreciable flux dissipation due to the penetration of vortices and anivortices at the opposite edges of the film and their subsequent annihilation in the middle of the strip. Since $B^{\perp}_{\rm self} \propto I$ we expect, as observed experimentally, a linear dependence of the threshold I on T because of the linear temperature dependencies of $B_{c2}(T)$ and $B_{c1}(T)$ near $T_c$and the flux-flow formula $\rho \approx \rho_n B/B_{c2} \propto I^*/B'_{c2}[1-T/T_c]$ leading to $I^* \propto -T$ for a fixed ρ, where $B'_{c2} = dH_{c2}/dT$ at $T = T_c$. As T is increased past T_{BKT}, the plasma of dissociated vortex-antivortex pairs that appears above T_{BKT} leads to a suppression in the order parameter and a consequent boost in the flux-flow resistivity. This may explain why the cross over between pair-breaking and self-flux-dissipation regimes appears to be tied to the BKT temperature.

The condition that the self-field at the edges exceeds $B_{c2}(T)$ gives currents well above the values observed in our experiments, so we suggest the following scenario of the crossover based on penetration of vortex semi-loops at the film edges. A rough estimate of the current level required to promote penetration of a vortex at the film edge can be obtained from the energy balance between the work of the Lorentz force $\simeq I\Phi_0 d/2w$ to form a vortex semi-loop of diameter equal to the film thickness d at the edge[11], and the self-energy of the vortex $\simeq \Phi^2 d/4\pi\mu_0\lambda^2$ at the film edge[12]. The condition $I\Phi_0 d/2w \simeq \Phi^2 d/4\pi\mu_0\lambda^2$ then yields $I = I_0(1-T/T_c)$. Here $I_0 \simeq w\Phi_0/2\mu_0\lambda^2(0) \approx 0.2$ A for $\lambda(0) = 124$ nm estimated below from our experimental data.

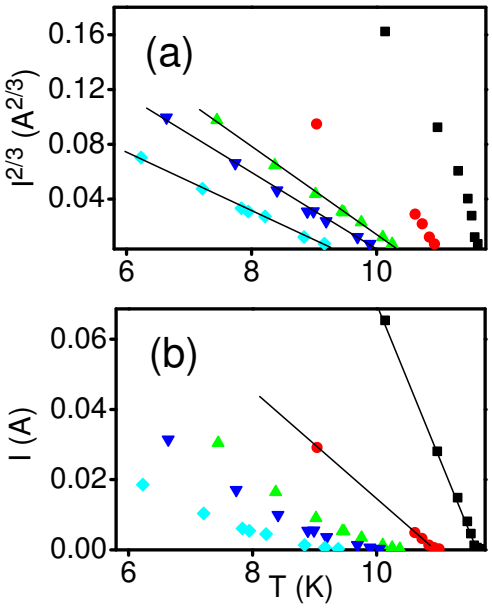

FIG. 2: *(a) Two-thirds power of the applied current versus the temperature for sample B for the following normalized-resistance criteria: R_c/R_n = 0.49, 0.62, 0.69, 0.81, and 0.92 (where R_n is the normal-state resistance). (b) The same applied-current data plotted linearly against the same temperatures as in panel (a). Straight lines are guides to the eye.*

Another window on current induced depairing is provided by high pulsed current-voltage characteristics at various fixed temperatures. As shown in Fig. 3(a) the current is able to drive the system completely normal at all temperatures. This provides one of the cleanest methods[13] for measuring the temperature dependence of the normal-state resistance $R_n(T)$ below the transition[19]. From Fig. 3(a), it is seen that R_n is approximately the same for the different temperatures. This is typical of metallic systems in which R_n tends to approach a constant residual value as $T \to 0$; however, our measurement is sensitive enough to detect small variations in $R_n(T)$,

which will be plotted and discussed later. The transition

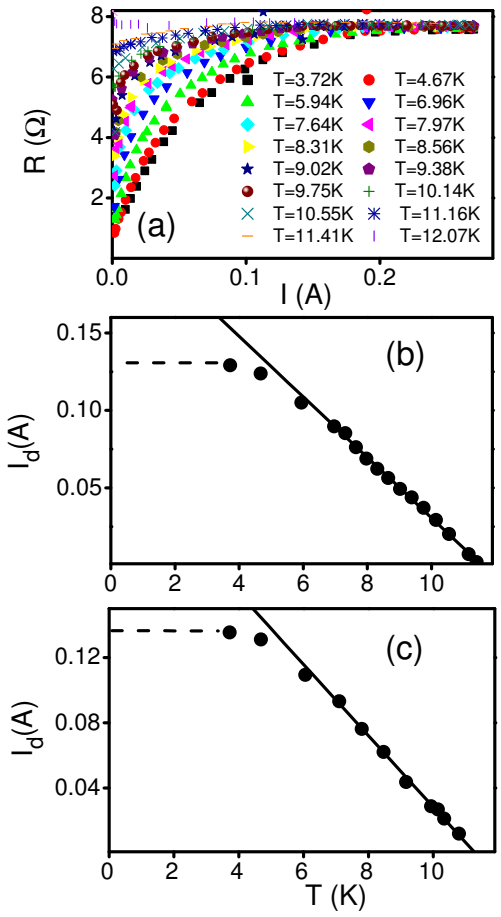

FIG. 3: *(a) Resistance vs current curves for sample A at various fixed temperatures. The plateaus, where the current ($I \gtrsim 0.2$ A) has completely destroyed the superconductivity, represent the normal resistances R_n for each T. (b) The resistive current I^*, defined at 90% of R_n for each T, versus temperature for sample A. The linear fit to the higher temperature data produces an intercept of $I_0 = 0.23$ A. The horizontal dashed line shows that the function tends to saturate to a value of $I_d(T \to 0) \gtrsim 0.131$ A at low temperature. (c) Similar $I^*(T)$ data for sample B, with $I_d(T \to 0) \gtrsim 0.136$ A. Here the linear fit extrapolates to an intercept of $I_0 = 0.25$ A.*

in $R(I)$ becomes rounded as $T \to T_c$ and naturally becomes flat and Ohmic for $T > T_c$. Here, we will define the "resistive critical current" I^* at a criterion of 90% of the R_n plateau, anticipating that $I^* \sim I_d$ as $T \to 0$, because this limit represents the current required to drive completely normal a fully condensed state. Fig. 3(b) and (c) show these measured $I^*(T)$ functions for samples A and B respectively. The observed intercepts of the linear portions, $I_0 = 0.23$ A and 0.25 A are consistent with the rough estimate of $I_0 \approx 0.2$ calculated earlier. The dashed horizontal lines in panels (b) and (c) provide the values $I_d(T \to 0) \gtrsim 0.131$ A and 0.136 A.

In order to obtain, more accurately, the intrinsic ρ_n and depairing current density j_d of the 7 nm thick superconducting interfacial layer itself, we need to subtract the small parallel current through the underlying FeTe. A separate measurement of pure FeTe deposited on ZnSe/GaAs, without the Bi_2Te_3 top layer, reveals the resistivity curve plotted in Fig. 4(a), which has an order of magnitude ($\sim 100\mu\Omega$-cm) that is characteristic of many of high-temperature superconductors. The corrected $j_d(T = 0)$ then works out to be 1.5×10^8 A/cm^2 for both samples, which is a typical value (j_d ranges 10^7–10^9 A/cm^2 for most superconductors). Similarly the R_n plateaus of Fig. 3(a) were corrected using the Fig. 4(a) function, which leads to the intrinsic $\rho_n(T)$ for the two samples shown in Fig. 4(b). This absolute value of $\rho_n(T \to 0) \sim 200$ nΩ-cm represents an extraordinarily conductive normal state for a superconducting system. This information will be analyzed below to see what can be learnt about the scattering rates, after obtaining information on the superfluid density and carrier concentration from j_d.

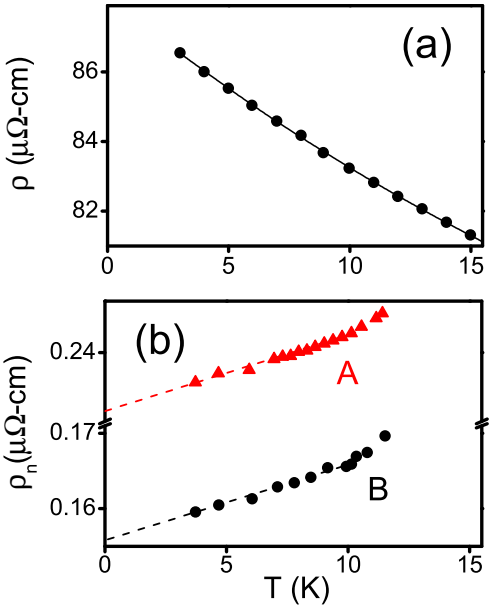

FIG. 4: *(a) Resistivity of pure FeTe deposited on ZnSe/GaAs without any Bi_2Te_3 top layer. (b) Intrinsic normal-state resistivity of the interface for samples A (red triangles) and B (black circles).*

Before using the results shown above to extract intrinsic microscopic characteristics of Bi_2Te_3/FeTe interfacial superconductor, we note that the combination of Bi_2Te_3 and FeTe band structures are likely to lead to multiple bands intersecting the Fermi level. As a result, extracting electronic parameters from experimental data generally requires formulas for j_d, H_{c2} and λ obtained for multiband superconductors[14,15]. However, using these formulas greatly increases the number of microscopic input parameters which are currently not known. In addition to electronic parameters in different bands, these include

at least four matrix elements of superconducting pairing constants, as well as other parameters which quantify the symmetry of the order parameter and details of microscopic pairing mechanism. To avoid these complications and to get a qualitative insight into electronic parameters of Bi_2Te_3/FeTe, we use a universal anisotropic Ginzburg-Landau (GL) theory, assuming only one dominant band. The values computed with these assumptions turn out to be self consistent, thus providing some justification for this approach.

We first use the anisotropic GL theory to extract the coherence lengths $\xi_\parallel(T)$ and $\xi_\perp(T)$, parallel and perpendicular to the interface respectively. From Ref. 2, we have a perpendicular-to-interface $B_{c2}^{\perp}(0) = \Phi_0/2\pi\xi_\parallel^2(0) \approx 17$ T and a parallel-to-interface $B_{c2}^{\parallel}(0) = \Phi_0/2\pi\xi_\parallel(0)\xi_\perp(0) \approx 40$ T, leading to an in-plane $\xi_\parallel(0) \approx 4.4$ nm and a perpendicular $\xi_\perp(0) \approx 1.9$ nm. Note that in an interface superconductor of thickness d, the formula $B_{c2}^{\parallel} = \Phi_0/2\pi\xi_\parallel\xi_\perp$ is applicable if $\xi_\perp(T) < d$, whereas near T_c where $\xi_\perp(T) > d$, we have $B_{c2}^{\parallel} = \Phi_0/2\pi\xi_\parallel d$. Our measured in-plane $j_d(0)$ can be related to the in-plane $\lambda_\parallel(0)$ and the perpendicular $B_{c2}^{\perp}(0)$ through[8] $j_d = (1/\mu_0\lambda^2)(2\Phi_0 B_{c2}/27\pi)^{1/2}$, which gives $\lambda_\parallel(0) = 124$ nm. The corresponding zero-T Pearl screening length[16] is $\Lambda(0) = 2\lambda^2/d = 4.4$ μm. As emphasized in our earlier work[5,17], the combination of B_{c2} and j_d provides a useful method for obtaining a single-band λ purely from transport measurements, which directly gives an absolute value of $\lambda(0)$ and is unaffected by magnetism in the material.

We now utilize the information obtained about λ and ρ_n to estimate the carrier concentration, Fermi surface parameters, and mean free path characterizing the normal state of the interface layer, using the effective single-band approximation mentioned above. From $\lambda^2(0) = m^*/\mu_0 n_s(0)e^2 \approx m/\mu_0 n e^2$ applicable in the clean limit at $T = 0$ we get $n \approx 1.8 \times 10^{21}$ per cm^3, assuming that the effective electron mass m^* equals the free electron mass, m, e is the electron charge, and the carrier concentration n equals the superfluid density n_s. In a two-band superconductor, the penetration depth would depend on intraband densities and effective masses, according to $\lambda^{-2} = e^2\mu_0(n_1/m_1 + n_2/m_2)$, where the indices 1 and 2 correspond to the respective bands[15]. The effective single-band value of n evaluated above is similar to n characteristic of high temperature superconductors and about 2 orders of magnitude lower than n in highly conductive metals such as copper. This low value of n together with the very high normal conductivity implies a rather long scattering time τ and mean-free-path l. The Fermi wave number for this n computes to $k_F(3D) = m^* v_F/\hbar = (3\pi^2 n)^{1/3} = 3.8 \times 10^9$ m^{-1} and $k_F(2D) = (2\pi n d)^{1/2} = 9.0 \times 10^9$ m^{-1} in three and two dimensions, respectively. In both cases the Fermi wavelength $\lambda_F = 2\pi/k_F \ll d$, validating the continuum approximation for states along the perpendicular direction and justifying the anisotropic 3D treatment of the normal state. Then from the Drude relationship $\rho \approx m/ne^2\tau$ we get $\tau \approx 10$ ps, which agrees well with the scattering rates ($\sim \hbar/0.05$ meV $= 13$ ps) measured by Pan et al.[18] using spin and angle resolved photoemission spectroscopy. Combining this value of τ with the Fermi velocity $v_F = \hbar k_F/m \approx 440$ km/s, we get $l = v_F\tau = 4.2$ μm. The very long l, which well exceeds d, indicates that scattering from the faces that bound the superconducting layer is of a specular nature.

There remain many open questions about this fascinating system and there may be other possible origins of the superconductivity besides the suggested doping effect, through charge transfer from the Bi_2Te_3 into FeTe. However, the information obtained in this work provides connections between some key superconducting and normal-state parameters, and it is hoped that this will provide a foundation for future research into this class of systems.

IV. ACKNOWLEDGMENTS

The work related to the measurements and analysis was supported by the U. S. Department of Energy through grant number DE-FG02-99ER45763. The work related to the synthesis of the films was supported by the Research Grants Council of the HKSAR under Grant No. 16305514.

* Corresponding author email: kunchur@sc.edu; URL: http://www.physics.sc.edu/~kunchur

[1] M. Z. Hasan and C. L. Kane, Rev. Mod. Phys **82**, 3045 (2010); X. L. Qi and S. C. Zhang, Rev. Mod. Phys **83**, 10571110 (2011); L. Fu and C. Kane, Phys. Rev. Lett **100**, 096407 (2008); H. Y. Hwang et al., Nat. Mater **11**, 103113 (2012); J. Pereiro, A. Petrovic, C. Panagopoulos, and I. Bozovic, Phys. Express **1**, 208241 (2011); E. Wang et al., Nature Physics **9**, 621 (2013); P. Zareapour et al., Phys. Rev. B **90**, 241106 (2014); T. Yilmaz, et al., Phys. Rev. Lett. **113**, 067003 (2014); J. Wang et al., Phys. Rev. B **85**, 045415 (2012).

[2] Q. L. He et al. Nature Communications **5**, 4247 (2014).

[3] M. N. Kunchur et al., unpublished.

[4] M. Q. He et al., arXiv:1407.5875 [cond-mat.supr-con].

[5] M. N. Kunchur, C. Dean, M. Liang, N. S. Moghaddam, A. Guarino, A. Nigro,G. Grimaldi, A. Leo, Physica C **495**, 66 (2013).

[6] M. N. Kunchur, D. K. Christen, C. E. Klabunde, and J. M. Phillips, Phys. Rev. Lett. **72**, 752 (1994).

[7] M. N. Kunchur, Sung-Ik Lee, and W. N. Kang, Phys Rev. B **68**, 064516 (2003).

[8] M. N. Kunchur, J. Phys.: Condens. Matter **16**, R1183-R1204 (2004).

[9] M. N. Kunchur, Mod. Phys. Lett. B. **9**, 399 (1995).
[10] G. F. Saracila and M. N. Kunchur, Phys. Rev. Lett. **102**, 077001 (2009).
[11] M. N. Kunchur, M. Liang, and A. Gurevich, Phys. Rev. B **86**, 024521 (2012).
[12] A. Gurevich and V. M. Vinokur, Phys. Rev. Lett. **100**, 227007 (2008)
[13] M. N. Kunchur, B. I. Ivlev, D. K. Christen, and J. M. Phillips, Phys. Rev. Lett. **84**, 5204 (2000).
[14] E. J. Nicol and J. P. Carbotte, Phys. Rev. B **72**, 014520 (2005).
[15] A. Gurevich, Rep. Prog. Phys. **74** 124501 (2011).
[16] J. Pearl, Appl. Phys. Lett. **5**, 65 (1964).
[17] M. Liang, M. N. Kunchur, L. Fruchter, Z.Z. Li, Physica C **492**, 178 (2013).
[18] Z.-H. Pan et al., Phys. Rev. Lett. 108, 187001 (2012).
[19] Techniques utilizing flux motion—which use the vortex core as a window to the normal state—require interpretation and modeling. Techniques utilizing high magnetic fields to drive the system normal are subject to magnetoresistance and may require prohibitively high magnetic fields. Compared with magnetoresistance, electroresistance—departure from Ohm's law at high current densities—is negligible in the normal state.